PAPER • OPEN ACCESS

# Response of the Southern Hemisphere extratropical cyclone climatology to climate intervention with stratospheric aerosol injection

ENVIRONMENTAL RESEARCH
CLIMATE

PAPER

# Response of the Southern Hemisphere extratropical cyclone climatology to climate intervention with stratospheric aerosol injection

**Michelle Simões Reboita**[1,*], **João Gabriel Martins Ribeiro**[1], **Natália Machado Crespo**[2], **Rosmeri Porfírio da Rocha**[3], **Romaric C Odoulami**[4], **Windmanagda Sawadogo**[5] and **John Moore**[6]

[1] Instituto de Recursos Naturais, Universidade Federal de Itajubá, Itajubá, Brazil
[2] Department of Atmospheric Physics, Faculty of Mathematics and Physics, Charles University, Prague 180 00, Czech Republic
[3] Instituto de Astronomia, Geofísica e Ciências Atmosféricas, Universidade de São Paulo, São Paulo, Brazil
[4] African Climate and Development Initiative, University of Cape Town, Cape Town, South Africa
[5] Institute of Geography, University of Augsburg, 86159 Augsburg, Germany
[6] Arctic Centre U. Lapland, Finland
[*] Author to whom any correspondence should be addressed.

**E-mail:** reboita@unifei.edu.br, gabrielmr472@unifei.edu.br, nataliacrespo@alumni.usp.br, rosmerir.rocha@iag.usp.br, romaric.odoulami@uct.ac.za, windmanagda.sawadogo@uni-a.de and john.moore.bnu@gmail.com

**Keywords:** stratospheric aerosol injection, solar radiation modification, extratropical cyclones, future projections, Southern Hemisphere

OPEN ACCESS

RECEIVED
25 February 2024

REVISED
24 April 2024

ACCEPTED FOR PUBLICATION
29 May 2024

PUBLISHED
20 June 2024



## Abstract

Little is known about how climate intervention through stratospheric aerosol injection (SAI) may affect the climatology of the Southern Hemisphere extratropical cyclones under warming scenarios. To address this knowledge gap, we tracked extratropical cyclones from 2015 to 2099 in a set of projections of three international projects: the Assessing Responses and Impacts of Solar Climate Intervention on the Earth System with Stratospheric Aerosol Injection (ARISE), the Stratospheric Aerosol Geoengineering Large Ensemble (GLENS), and the Geoengineering Model Intercomparison Project (GeoMIP/G6sulfur). Comparisons were performed between no-SAI and SAI scenarios as well as between different timeslices and their reference period (2015–2024). Among the findings, both no-SAI and SAI project a decrease in cyclone frequency towards the end of the century although weaker under SAI scenarios. On the other hand, cyclones tend to be stronger under no-SAI scenarios while keeping their intensity more similar to the reference period under SAI scenarios. This means that under SAI scenarios the climatology of cyclones is less affected by global warming than under no-SAI. Other features of these systems, such as travelling distance, lifetime, and mean velocity show small differences between no-SAI and SAI scenarios and between reference and future periods.

## 1. Introduction

Extratropical cyclones are a response of the atmosphere to attain thermal equilibrium. They develop mainly due to near-surface horizontal temperature gradients, a predominant feature in mid-latitudes, and transport heat and water vapor towards the poles and cold and dry air towards the tropics (Peixoto and Oort 1992). Despite their important role in the climatic system, many cyclones can also cause extreme weather events such as intense precipitation, strong winds, and abrupt temperature changes. Over the ocean, air-sea momentum exchange is responsible for maritime agitation, which can lead to the occurrence of storm surges and giant waves, causing disruptions to navigation, operations on oil platforms, and the destruction of coastal ecosystems and infrastructure (Rocha *et al* 2004, Gramcianinov *et al* 2020, Faria *et al* 2023).

In extensive databases, such as reanalysis and model outputs, cyclone climatologies are obtained using objective methods based on the mean sea level pressure (MSLP), relative vorticity, or geopotential height (Walker *et al* 2020). For the Southern Hemisphere, centenary reanalysis (ERA20C) from 1900 to 2010

indicates a negative trend in the frequency of extratropical cyclones (Marrafon *et al* 2021). This signal is also projected in future warming scenarios by global and regional climate models (Bengtsson *et al* 2009, Michaelis *et al* 2017, Sinclair *et al* 2020, de Jesus *et al* 2021, Reboita *et al* 2021a, Priestley and Catto 2022). In contrast, the frequency of stronger cyclones (systems that reach central pressure lower than 980 hPa in some period of their lifecycle) increases in reanalyses (Pezza and Ambrizzi 2003, Reboita *et al* 2015) and in climate projections (Reboita *et al* 2015, 2021a). For instance, along the eastern coast of South America the frequency of explosive cyclones (i.e. cyclones with pressure dropping by ∼24 hPa/24 h) is projected to increase mainly near Uruguay and south of Brazil (Reboita *et al* 2021b), which can cause even more damage to coastal areas.

Despite significant progress in understanding the role of climate change in the climatology of extratropical cyclones, there is a lack of studies focusing on the impact of climate intervention on these systems. Climate intervention (also known as climate geoengineering) appears as an aggressive approach to reduce global warming since the climate system is intentionally modified. It involves deliberate manipulation of the physical, chemical, or biological processes of the Earth system with the intention of tempering the harmful effects of anthropogenic greenhouse gas emissions (AMS. American Meteorological Society 2022). Climate intervention encompasses two categories: (1) removing $CO_2$ from the atmosphere, known as carbon dioxide removal (CDR), and (2) reflecting sunlight, known as solar radiation modification (SRM) or solar geoengineering. One of SRM approaches involves the injection of sulfate aerosols (or their precursor sulfur dioxide—$SO_2$) into the stratosphere to enhance solar energy reflection; this approach is known in the literature as stratospheric aerosol injection (SAI). By reducing the amount of solar energy entering the climate system, the Earth's surface would cool on average. This concept draws from observations of past volcanic eruptions. For instance, the eruption of Mount Pinatubo in 1991 injected 20 million tons of $SO_2$ into the stratosphere, resulting in increased sunlight reflection and a globally averaged surface air temperature cooling of ∼0.3 °C for a period of 3 years (National Research Council 2015).

Both categories of climate intervention present risks and deserve much study before their real application (Robock *et al* 2009, Dykema *et al* 2014, National Research Council 2015, AMS. American Meteorological Society 2022, Ricke *et al* 2023). One way to assess the impact of climate intervention approaches on the climate system (basic variables and atmospheric systems) is through climate simulations/projections. Three international projects have conducted simulations/projections by using SAI and have made the data available: the Assessing Responses and Impacts of Solar Climate Intervention on the Earth System with Stratospheric Aerosol Injection (ARISE; Richter *et al* 2022), the Stratospheric Aerosol Geoengineering Large Ensemble (GLENS; Tilmes *et al* 2018), and the Geoengineering Model Intercomparison Project (GeoMIP) with the experiment G6sulfur; Visioni *et al* 2021). These experiments have some differences such as the simulated period, greenhouse gas scenarios, and the region where the particles are introduced in the stratosphere (Irvine *et al* 2016); more details about them are provided in section 2. Currently, the data of these three projects are largely used for assessing the potential impact of SAI on the climate system (e.g. Bednarz *et al* 2022, Camilloni *et al* 2022, Patel *et al* 2023).

While a general result is that SAI could effectively limit global warming (Moore *et al* 2015, Irvine *et al* 2019, Krishnamohan *et al* 2019), the impacts on various aspects of the climate system, such as in water balance and in the lifecycle of the atmospheric systems, remain unclear due to the different stratospheric processes and formulations of $SO_2$ injection in climate models (Kravitz *et al* 2014, Jiang *et al* 2019). For instance, Ricke *et al* (2023) reported that 'The expected hydrological effects of reducing insolation are among the most uncertain and consequential impacts of solar geoengineering'.

In terms of atmospheric systems without considering SAI, Chand *et al* (2022) found a negative trend in the frequency of tropical cyclones across all ocean basins using centenary reanalysis. This trend is also consistent in climate projections under warming scenarios, along with an increase in the tropical cyclone's intensity (Vecchi and Soden 2007, Walsh *et al* 2015). Under SAI scenarios, studies such as that of Jones *et al* (2017) have shown that aerosol enhancements confined to a single hemisphere could effectively modulate the North Atlantic tropical cyclone activity. For instance, sulfate SAI in the Southern Hemisphere would enhance tropical cyclone frequency relative to global aerosol injection, and vice-versa for injection in the Northern Hemisphere.

Specifically for extratropical cyclones, the authors do not know of studies applying the identification and tracking of individual cyclones aiming to compare scenarios with and without SAI. Until this date, the only two published studies on extratropical cyclones analyzed environmental conditions: one based on mean available potential energy (Gertler *et al* 2020) and the other on Rossby wave packets (Karami *et al* 2020). Gertler *et al* (2020) investigated scenarios with continued preindustrial conditions, $4xCO_2$, and $4xCO_2$ plus SAI from GeoMIP. Under $4xCO_2$, storm tracks in the Northern Hemisphere are projected to weaken somewhat and greatly strengthen in the Southern Hemisphere. On the other hand, under the climate intervention scenario the storm tracks weaken in both hemispheres, but in the Northern Hemisphere the weakening is comparable to that from $4xCO_2$. Karami *et al* (2020) investigated the storm track response to

**Table 1.** Mean characteristics of the three projects. The used period in the study is indicated by *. In the rows 'Ensemble size' the numbers in brackets indicate the members available online. For instance, GLENS no-SAI has 20 members from 2010 to 2030 but only the realizations 001, 002 and 003 are available.

| | ARISE | GLENS | GeoMIP/G6sulfur |
|---|---|---|---|
| Model version | CESM2(WACCM6) | CESM1(WACCM5) | MPI-ESM-LR |
| Main reference | Richter *et al* (2022)<br>Hueholt *et al* (2023) | Tilmes *et al* (2018)<br>Hueholt *et al* (2023) | Wieners *et al* (2019)<br>Niemeier *et al* (2019)<br>Visioni *et al* (2021) |
| Spatial resolution (longitude/latitude) | 1.25° × 0.9° | 1.25° × 0.9° | 1.875° × 1.85° |
| Calendar | 365 d | 365 d | 365/366 d*<br>*February 29 is removed |
| Ensemble size (no-SAI) | 5 members 2015–2069*<br>5 members 2015–2100 (it does not have 6-hourly data) | 20 members 2010–2030 (001–003)<br>3 members 2010–2097* (004–020) | 3 members 2015–2100* (r1i1p1f1, r2i1p1f1, r3i1p1f1) |
| Ensemble size (SAI) | 10 members 2035–2069* | 20 members 2015–2099* (001–020) | 3 members 2015–2100* (r1i1p1f1, r2i1p1f1, r3i1p1f1) |
| Forcing scenario | SSP2-4.5: Moderate mitigation | RCP8.5: No mitigation | SSP5-8.5: No mitigation |
| Global mean surface temperature target | 2020–2039 average of first 5 SSP2-4.5 members (≈1.5 °C above pre-industrial) | 2015–2024 average of first 13 RCP8.5 members (≈1.1 °C above pre-industrial) | Reduce the globally averaged surface temperature down to the SSP2-4.5 level |
| SAI deployment year | 2035 | 2020 | 2020 |
| Injection height | ≈21 km | ≈25 km | Between 18 and 20 km |
| Injection sites | 30° and 15°N/S, all at 180°E | 30° and 15°N/S, all at 180°E | Continuous from 10 °N—10 °S all at Greenwich meridian |
| Injection intensity rate | Linear increase from 0.5 Tg-SO2 per year | 0.55 Tg-SO2 per year | 0.6 Tg-SO2 per year |
| Injection amount | ≈10 Tg-SO2 $yr^{-1}$ (2069) | ≈50 Tg-SO2 $yr^{-1}$ (2099) | 36 Tg-SO2 $yr^{-1}$ (2100) |
| Injection duration | 2035–2069 (34 years) | 2020–2099 (79 years) | 2020–2100 (80 years) |

the RCP8.5 scenario and to this same scenario plus sulfate SAI over the Middle East and North Africa region between 2050 and 2070. They compared GLENS projections with the present climate, and the main findings are: (a) increasing greenhouse gas concentrations result in the northward (poleward) shift of the storm tracks in all seasons, (b) under SAI scenario, there is a partial offset of the poleward shift of the storm tracks seen in the RCP8.5, consequently contributing to reducing the precipitation in the study area.

As at mid-latitudes the weather is primarily controlled by the development of extratropical cyclones and their associated fronts (Catto and Pfahl 2013, Eisenstein *et al* 2023), it is crucial to explore the consequences of SAI on the climatology of these systems under warming scenario using a different approach from the previously described studies. Hence, this study aims to address the existing research gap by assessing how the main features of extratropical cyclone's climatology (frequency, intensity, trajectory, etc) over the Southern Hemisphere could change in the future under SAI scenarios provided by ARISE, GLENS, and GeoMIP/G6sulfur projects.

## 2. Methodology

### 2.1. Study area and data

The study area encompasses the latitudes southern 20S to avoid the inclusion of tropical cyclones in the climatology (Reboita *et al* 2015). Extratropical cyclones are identified using MSLP at every 6 h (0000, 0600, 1200 and 1800 UTC) from three climate modeling projects: ARISE, GLENS, and GeoMIP/G6sulfur (table 1).

ARISE projections were carried out with CESM2 global climate model (GCM), GLENS with CESM1 and GeoMIP/G6sulfur with MPI-ESM1-2-LR (table 1). From each GCM we obtained three members without $SO_2$ SAI (hereafter called no-SAI) and with $SO_2$ SAI (hereafter called SAI). As these projections are well-documented in the literature, just a summary of their main information (such as number of members and design of the experiments) is provided here. Considering the no-SAI projections, they follow different

emission pathways, i.e. ARISE is under SSP2-4.5, GLENS is under RCP8.5 and GeoMIP is under SSP5-8.5 (hereafter $ARISE_{SSP2\text{-}4.5}$, $GLENS_{RCP8.5}$ and $GeoMIP_{SSP5\text{-}8.5}$). Although SAI projections in ARISE are named by ARISE-SAI-1.5 and in GeoMIP we are just using the G6sulfur experiment, in the present study, for brevity, we call these dataset only by $ARISE_{SAI}$, $GLENS_{SAI}$ and $GeoMIP_{SAI}$. In the three projects, SAI projections consider the $SO_2$ injection into the lower stratosphere at four off-equatorial locations (30 °S, 15 °S, 15 °N, and 30 °N) in $ARISE_{SAI}$ and $GLENS_{SAI}$, and within a range of 10°N and 10°S across the single longitude band of 0° in GeoMIP-SAI. Injection amounts at each latitude in the three experiments are controlled by a feedback algorithm, which aims to maintain the global mean surface temperature and its equator-to-pole and inter-hemispheric gradients at the baseline levels (Kravitz *et al* 2017). In $ARISE_{SAI}$ the baseline period was defined as the 2020–2039 mean, corresponding to the likely period when the real world will reach 1.5 K above pre-industrial conditions (Tebaldi *et al* 2021, MacMartin *et al* 2022). In $GLENS_{SAI}$, the baseline period used in the feedback algorithm was 2010–2030 mean.

As the projects differ in relation to the greenhouse gas emission scenarios (table 1), it leads to a different magnitude of SAI (Richter *et al* 2022), and also a distinct spatial distribution of the aerosols in the simulations (Bednarz *et al* 2022, Fasullo and Richter 2022). For instance, Bednarz *et al* (2022) compared the distribution of $SO_2$ injections in $ARISE_{SAI}$ and $GLENS_{SAI}$ and found that $GLENS_{SAI}$ has the largest concentrations of sulfate in the North Hemisphere tropics while $ARISE_{SAI}$ in the Southern Hemisphere tropics (the physical explanation for these differences are discussed in Fasullo and Richter 2022). Bednarz *et al* (2022) also highlight that larger injection rates are needed in $GLENS_{SAI}$ to reach the same amount of global cooling as in $ARISE_{SAI}$ or to offset the end of the century RCP8.5 scenario.

All GCMs provide data with horizontal resolution of 1.25° longitude ×0.9° latitude, except MPI-ESM-LR (1.875° longitude × 1.85° latitude). We highlight that one limitation of this study is the availability of projections with 6-hour frequency needed to track cyclones. The data used here were the ones available when this study started. Since the focus of this study is on extratropical cyclones, which are synoptic systems (horizontal dimension on the order of $10^3$ km), the horizontal resolution of the datasets do not need to be high. Thus, all projections were interpolated to 1.5° longitude ×1.5° latitude using the bi-linear interpolation method (Wahab 2017, Cerlini *et al* 2020). The ensemble mean for each model will be used since each project has considerable differences. Hence, it can be expected that the different projects would lead to differences in the spatial pattern of the extratropical cyclones' characteristics.

### 2.2. Extratropical cyclone tracking

Cyclones were identified and tracked using 6 hourly MSLP data with an objective method (algorithm) developed by Murray and Simmonds (1991a, 199b) and updated by Simmonds and Murray (1999) and Simmonds *et al* (1999). This algorithm has demonstrated reliable results in studies of extratropical cyclones over the Southern Hemisphere (Pezza and Ambrizzi 2003, Neu *et al* 2013, Reboita *et al* 2015, Grieger *et al* 2018).

Initially, the algorithm interpolates the MSLP from a regular (latitude-longitude) grid to a polar stereographic grid centered on the South Pole using the bicubic spline method, which eliminates anisotropy (it ensures that the grid resolution is uniform in all directions, mainly in the pole, Simmonds *et al* 2003). Next, the Laplacian of pressure ($\nabla^2 p$) for each grid point is calculated. Grid points candidate to be a cyclone are identified where there is a local maximum of $\nabla^2 p$ (which is associated with the minimum pressure) compared to that of the surrounding eight grid points. This process is carried out for all timesteps, and only systems with $\nabla^2 p$ exceeding 0.2 hPa $(\text{lat})^{-2}$ are considered for the following analyses (Simmonds and Murray 1999). Once the algorithm has identified the candidate grid points to be cyclones in all timesteps, it is necessary to connect these points over a sequence of timesteps to track the systems. This procedure comprises three stages (Simmonds *et al* 1999): (a) predicting the subsequent position of each low-pressure center, (b) calculating the probability of an identification between the predicted cyclone and each cyclone identified at the new timestep (identified with $\nabla^2 p$), and (c) defining the position of the minimum of pressure in the new timestep based on the highest probability of association obtained in stage (b). In summary, the tracking procedure is based on projecting cyclone positions from one analysis time to the next and comparing the projected positions with those of the cyclone analysis at the new time (Simmonds and Murray 1999).

The algorithm provides the central pressure and $\nabla^2 p$ for each timestep of a cyclone's trajectory (latitude and longitude). The $\nabla^2 p$ (calculated between the center of the system and the neighborhood) can be taken as measure of the strength of the cyclone, and values greater than 0.7 hPa $(°\text{lat})^{-2}$ are classified as strong systems, while values between 0.7 and 0.2 hPa $(°\ \text{lat})^{-2}$ are considered weak (Simmonds and Murray 1999). Knowing the cyclone trajectories, the algorithm is able to create a grid with some statistical quantities computed over different time scales (monthly, seasonal, yearly etc) as specified by the user. These statistics are trajectory density (SD), central pressure (CP), radius (R0), and depth (DP) of cyclones. The SD corresponds to the normalized number of systems passing through a given area, which is calculated by

summing contributions from all sampled positions (recorded along the tracks) and normalizing by an area of $10^3$ (degrees latitude)$^2$. CP represents the minimum pressure at the center of the cyclones, R0 indicates the distance between the cyclone center and the location where $\nabla^2 p = 0$, and DP is also a measure of cyclone strength. Although there is an expression to compute DP (see Simmonds *et al* 2003), it can be understood as the MSLP difference between the center and the region of the system with $\nabla^2 p = 0$ (cyclone external border); the values given by this variable are positive. Further details about these quantities are provided in Lim and Simmonds (2002). In this study, we computed the statistics on an annual basis.

### 2.3. Analyses

Extratropical cyclones were identified in each member of ARISE, GLENS, and GeoMIP/G6sulfur no-SAI and SAI projections. Climatologies were calculated using only cyclones with a lifetime equal to or greater than 24 h, and presented in terms of ensemble mean. Cyclone frequency is defined as the number of systems per month, season (DJF, MAM, JJA and SON) and year.

Trends and their statistical significance ($\alpha = 0.05$), using Sen's slope and Mann–Kendall test (Mann 1945, Kendall 1975), respectively, were calculated for the annual time series (2015–2099) of cyclone frequency, initial pressure, minimum pressure along the lifecycle, lifetime, travelling distance, and mean velocity. The t-test at the 0.05 significance level (Wilks 2020) was conducted to determine whether differences exist between the averages of the no-SAI and SAI scenarios at the same timeslice.

As shown in table 1, not all projects have data before 2015. Hence, we considered the period 2015–2024 from no-SAI projections as the reference period. This allows us to analyze the difference between the future timeslices (2040–2059, and 2080–2099) and the current period (2015–2024). In addition, the differences between the no-SAI and SAI scenarios are analyzed for annual mean features of the cyclones and displayed in maps. In these maps, significance statistical tests for mean difference are not included due to the weakness of the tests for cyclone's properties on the grid, as these systems have high variability in space and time (Pezza *et al* 2008, 2012, Catto *et al* 2011, Reboita *et al* 2015, Gentile *et al* 2023).

## 3. Results and discussions

### 3.1. Trends

The annual frequency of extratropical cyclones over the Southern Hemisphere from 2015 to 2099 in each ensemble is depicted in figure 1(a). Additionally, to provide a view of the spread among the members of each project, the minimum and maximum annual frequency identified for no-SAI and SAI scenario members are shown. Up to 2050, the ensembles do not indicate a large difference in the annual frequency of cyclones between the no-SAI and SAI scenarios. However, from the 2050-decade, SAI scenarios indicate a higher number of systems (figure 1(a)), contributing to a smoother negative trend, and even positive one in $\text{GLENS}_{\text{SAI}}$, when compared with that from no-SAI scenarios (table 2). The negative trends under no-SAI scenarios are consistent with the findings in the literature (Bengtsson *et al* 2009, de Jesus *et al* 2021, Reboita *et al* 2021a, Priestley and Catto 2022, Xu *et al* 2023). Table 2 reveals that, except for $\text{ARISE}_{\text{SAI}}$ and $\text{GLENS}_{\text{SAI}}$ projections, all the others exhibit statistically significant trends. In general, under the SAI scenarios, the frequency of extratropical cyclones is higher than under no-SAI scenarios and also higher than in the reference period (2015–2024), except in $\text{GeoMIP}_{\text{SAI}}$ (table 3). When the t-test is applied to identify whether the averages between the no-SAI and SAI scenarios at the same timeslice are statistically different, most timeslices and projects present statistically significant differences except for $\text{GeoMIP}_{\text{SSP5-8.5/SAI}}$ in 2060–2069 and 2080–2089 (table 3).

In future warming scenarios, the decrease in the frequency of extratropical cyclones is related to many interacting processes resulting in a complex picture. These include tropical upper-tropospheric warming (Kumar *et al* 2022), which leads to an expansion of the Hadley cell and, consequently, a poleward expansion of the regions with higher MSLP and subtropical anticyclones (Reboita *et al* 2019); polar near-surface warming, which leads to the weakening of the horizontal temperature gradients and, consequently, baroclinicity in mid-latitudes (Frederiksen *et al* 2016) resulting in the poleward migration of the storm tracks; increasing the amplitude of large waves and decreasing the amplitude of short waves (synoptic waves; Schemm and Röthlisberger 2024), further negatively affecting near-surface cyclogenesis. It is suggested that with the decrease in global warming caused by SAI, these processes will undergo fewer changes and consequently affect cyclones less. However, additional investigation of these mechanisms is necessary and is beyond the scope of this study.

The trend of the annual mean of the central MSLP during cyclogenesis and the minimum pressure (cyclone deepest phase across its lifecycle) are presented in figures 1(b) and (c), respectively. In both figures, the no-SAI scenarios project a negative and statistically significant trend (table 2), indicating that cyclones will be deeper in the future since lower central pressure is the main indicator of more intense cyclones. For

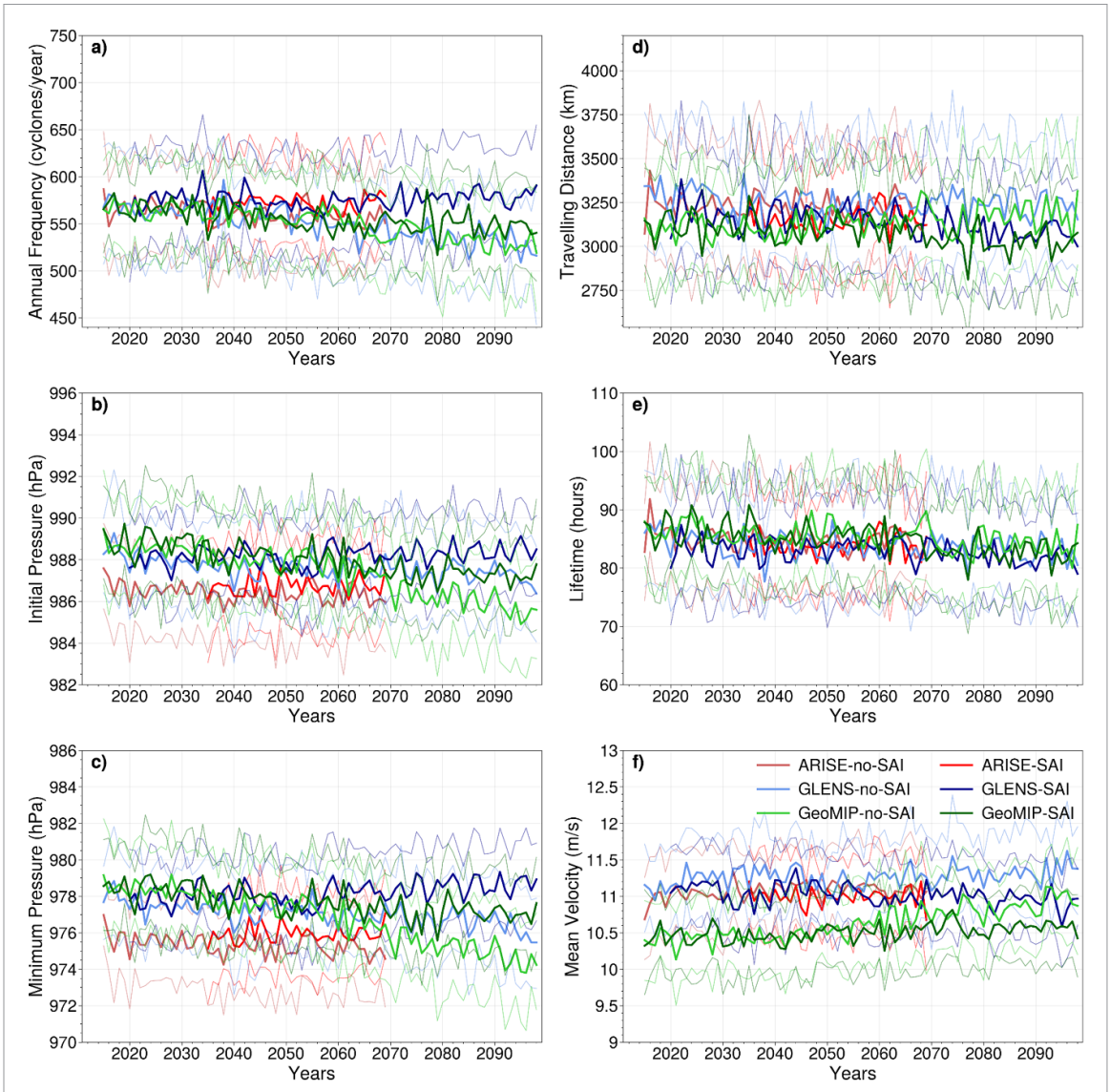


**Figure 1.** Extratropical cyclone trends over the Southern Hemisphere under no-SAI and SAI scenarios from 2015 to 2099: (a) annual frequency (number per year), (b) initial pressure (registered in the cyclogenesis, hPa), (c) minimum pressure during the whole lifecycle (hPa), (d) travelling distance (km), (e) lifetime (hours), and (f) mean velocity (m $s^{-1}$). Bold lines indicate the ensemble mean and light lines indicate the minimum and maximum values obtained by the members of each ensemble.

**Table 2.** Slope of the trends calculated for the annual time series (slope $year^{-1}$) of each ensemble shown in figure 1. Trends statistically significant at the level of $\alpha = 0.05$ are highlighted in bold.

| Project | Annual frequency | Initial pressure | Minimum pressure | Travelling distance | Lifetime | Mean velocity |
|---|---|---|---|---|---|---|
| $ARISE_{SSP2\text{-}4.5}$ | **−0.282** | **−0.011** | **−0.014** | −0.301 | −0.022 | **0.002** |
| $ARISE_{SAI}$ | −0.016 | 0.004 | 0.008 | 0.600 | 0.034 | 0.000 |
| $GLENS_{RCP8.5}$ | **−0.563** | **−0.012** | **−0.018** | **−0.816** | **−0.028** | **0.002** |
| $GLENS_{SAI}$ | 0.102 | **0.005** | **0.012** | **−1.651** | **−0.027** | **−0.002** |
| $GeoMIP_{SSP5\text{-}8.5}$ | **−0.548** | **−0.042** | **−0.054** | **1.353** | **−0.038** | **0.008** |
| $GeoMIP_{SAI}$ | **−0.286** | **−0.024** | **−0.021** | **−1.421** | **−0.057** | **0.002** |

instance, $GeoMIP_{SSP5\text{-}8.5}$ scenario indicates that the cyclones at the end of the century will be 3.1 and 4.0 hPa stronger for initial pressure (table 4) and minimum pressure (table 5), respectively, than in the present climate. Under SAI scenarios, the $ARISE_{SAI}$ and $GLENS_{SAI}$ project a positive trend in MSLP (figures 1(b) and (c)), corresponding to weaker systems in the future (table 2). Only $GeoMIP_{SAI}$ projects a negative trend, but it has a smoother slope compared to the no-SAI scenario (table 2). Tables 4 and 5 also indicate that in all timeslices cyclones are weaker under the SAI compared to no-SAI scenarios (in other words, MSLP is higher in SAI scenarios) and the differences are statistically significant. This is also noted when comparing the timeslices of SAI scenarios with the reference period; only $GLENS_{SAI}$ projects systems slightly deeper than in the reference period.

**Table 3.** Mean annual frequency of extratropical cyclones over the Southern Hemisphere obtained by the ensemble of no-SAI and SAI scenarios from ARISE-SAI, GLENS and GeoMIP for different timeslices. The asterisk (*) indicates that the difference between no-SAI and SAI averages in the same timeslice is statistically significant at the level of 0.05.

| | Project | 2015–2024 | 2060–2069 | 2070–2079 | 2080–2089 | 2090–2099 |
|---|---|---|---|---|---|---|
| Annual frequency (cyclones/year) | $ARISE_{SSP2-4.5}$ | 565.3 | 554.8 | — | — | — |
| | $ARISE_{SAI}$ | — | 573.0 * | — | — | — |
| | $GLENS_{RCP8.5}$ | 566.5 | 544.9 | 537.4 | 534.4 | 525.5 |
| | $GLENS_{SAI}$ | — | 574.1 * | 576.9 * | 580.2 * | 578.7 * |
| | $GeoMIP_{SSP5-8.5}$ | 565.1 | 543.2 | 543.7 | 531.2 | 528.9 |
| | $GeoMIP_{SAI}$ | — | 548.8 | 548.5 | 550.5 * | 545.5 * |

**Table 4.** Similar to table 3 but for initial pressure (hPa).

| | Project | 2015–2024 | 2060–2069 | 2070–2079 | 2080–2089 | 2090–2099 |
|---|---|---|---|---|---|---|
| Initial pressure (hPa) | $ARISE_{SSP2-4.5}$ | 986.6 | 986.2 | — | — | — |
| | $ARISE_{SAI}$ | — | 986.8 * | — | — | — |
| | $GLENS_{RCP8.5}$ | 988.2 | 978.6 | 987.4 | 987.5 | 987.0 |
| | $GLENS_{SAI}$ | — | 988.3 * | 988.3 * | 988.4 * | 988.5 * |
| | $GeoMIP_{SSP5-8.5}$ | 988.6 | 987.4 | 986.2 | 986.1 | 985.5 |
| | $GeoMIP_{SAI}$ | — | 987.7 | 987.2 * | 987.4 * | 987.3 * |

**Table 5.** Similar to table 3 but for minimum pressure along the cyclone's lifetime (hPa).

| | Project | 2015–2024 | 2060–2069 | 2070–2079 | 2080–2089 | 2090–2099 |
|---|---|---|---|---|---|---|
| Minimum pressure (hPa) | $ARISE_{SSP2-4.5}$ | 975.6 | 975.0 | — | — | — |
| | $ARISE_{SAI}$ | — | 976.0 * | — | — | — |
| | $GLENS_{RCP8.5}$ | 977.8 | 977.0 | 976.7 | 976.8 | 976.0 |
| | $GLENS_{SAI}$ | — | 978.3 * | 978.5 * | 978.6 * | 978.7 * |
| | $GeoMIP_{SSP5-8.5}$ | 978.4 | 976.6 | 975.4 | 975.1 | 974.4 |
| | $GeoMIP_{SAI}$ | — | 977.5 * | 976.9 * | 977.3 * | 977.0 * |

**Table 6.** Similar to table 3 but for travelling distance (km).

| | Project | 2015–2024 | 2060–2069 | 2070–2079 | 2080–2089 | 2090–2099 |
|---|---|---|---|---|---|---|
| Travelling distance (km) | $ARISE_{SSP2-4.5}$ | 3251.5 | 3222.3 | — | — | — |
| | $ARISE_{SAI}$ | — | 3161.7 | — | — | — |
| | $GLENS_{RCP8.5}$ | 3305.7 | 3232.5 | 3262.2 | 3230.9 | 3237.9 |
| | $GLENS_{SAI}$ | — | 3144.4 * | 3118.3 * | 3063.6 * | 3082.7 * |
| | $GeoMIP_{SSP5-8.5}$ | 3113.1 | 3190.5 | 3118.9 | 3194.9 | 3185.9 |
| | $GeoMIP_{SAI}$ | — | 3083.6 * | 3032.4 | 3012.7 * | 3035.1 * |

It appears controversial that with a decrease in baroclinicity in warming scenarios, extratropical cyclones can exhibit greater intensity. However, as shown in the literature, this is a consequence of higher moisture availability contributing to diabatic processes in the cyclone's environment (Catto *et al* 2019, Kodama *et al* 2019, Sinclair *et al* 2020, Reboita *et al* 2021b).

While there is a clear signal regarding future trends for the aforementioned variables, there are more uncertainties concerning traveling distance. While $ARISE_{SSP2-4.5}$ and $GLENS_{RCP8.5}$ scenarios project a negative trend for the travelling distance, $GeoMIP_{SSP5-8.5}$ projects a positive one. On the other hand, $ARISE_{SAI}$ and $GeoMIP_{SAI}$ have opposite trends compared with no-SAI scenarios, and $GLENS_{SAI}$ projects a more intense negative trend than under no-SAI. Only $ARISE_{SSP2-4.5/SAI}$ does not have a statistically significant trend (table 2). As shown in table 6, cyclone's travel distances range between 3000 and 3300 km, indicating a small mean difference of only 300 km (10%) in the trajectory of the cyclones. Nevertheless, the differences are statistically significant, except in 2060–2069 for $ARISE_{SSP2-4.5/SAI}$ and in 2070–2079 for $GeoMIP_{SSP8-8.5/SAI}$ (table 6).

Extratropical cyclones exhibit a negative trend in their lifetime, but that does not exceed ∼4 h (4% of their total duration) between the reference period and the end of the century in both no-SAI and SAI scenarios (figure 1(e)). Despite this small value, the trends are statistically significant, except for the $ARISE_{SSP2-4.5/SAI}$ scenarios (table 2). Under SAI scenarios although cyclones are less deep (table 5) their duration seems not to be affected (table 7).

As mean velocity is a relation between traveling distance and lifetime, the small changes projected for both variables throughout the future (tables 6 and 7) result in small changes in mean velocity (figure 1(f) and

**Table 7.** Similar to table 3 but for cyclone's lifetime (hours).

| | Project | 2015–2024 | 2060–2069 | 2070–2079 | 2080–2089 | 2090–2099 |
|---|---|---|---|---|---|---|
| Lifetime (h) | $ARISE_{SSP2-4.5}$ | 86.0 | 84.7 | — | — | — |
| | $ARISE_{SAI}$ | — | 83.9 | — | — | — |
| | $GLENS_{RCP8.5}$ | 85.8 | 83.2 | 83.6 | 83.2 | 82.9 |
| | $GLENS_{SAI}$ | — | 83.2 | 82.6 | 81.6 | 81.8 |
| | $GeoMIP_{SSP5-8.5}$ | 86.8 | 86.4 | 83.1 | 84.6 | 83.7 |
| | $GeoMIP_{SAI}$ | — | 85.2 | 82.8 | 82.7 | 82.7 |

**Table 8.** Similar to table 3 but for mean velocity (m $s^{-1}$).

| | Project | 2015–2024 | 2060–2069 | 2070–2079 | 2080–2089 | 2090–2099 |
|---|---|---|---|---|---|---|
| Mean velocity (m $s^{-1}$) | $ARISE_{SSP2-4.5}$ | 11.0 | 11.0 | — | — | — |
| | $ARISE_{SAI}$ | — | 11.0 | — | — | — |
| | $GLENS_{RCP8.5}$ | 11.1 | 11.3 | 11.3 | 11.3 | 11.4 |
| | $GLENS_{SAI}$ | — | 11.0 * | 11.0 * | 11.0 * | 10.9 * |
| | $GeoMIP_{SSP5-8.5}$ | 10.4 | 10.7 | 10.8 | 10.8 | 11.0 |
| | $GeoMIP_{SAI}$ | — | 10.5 * | 10.6 * | 10.6 * | 10.6 * |

table 8). The maximum difference between SAI and no-SAI scenarios is 0.5 m $s^{-1}$ in $GLENS_{RCP8.5/SAI}$ in 2090–2099 (table 8), which implies slower cyclones under SAI scenario. Although trends are not visually apparent in figure 1(f), the calculated trend slope reveals a positive and statistically significant trend for all datasets except for the $ARISE_{SAI}$, which shows no trend, and the $GLENS_{SAI}$, which exhibits a negative and significant trend (table 2). In table 8, the t-test for average differences between the scenarios only indicated no significance for $ARISE_{SSP2-4.5/SAI}$.

Overall, the slight changes projected for travelling distance, lifecycle, and mean velocity until the end of the century under no-SAI scenarios are consistent with findings from studies, such as Reboita *et al* (2021b) and Sinclair *et al* (2020).

### 3.2. Annual cycle

The annual cycle of extratropical cyclones in both scenarios considering two periods (2040–2059 and 2080–2099) is shown in figure 2. There is a high frequency of cyclones between May and August, which is the period with higher baroclinicity in the Southern Hemisphere (Holton 2004, Frederiksen *et al* 2016) and an important cyclogenesis driver. In December, the frequency of cyclones reaches a minimum, which is followed by another one in February. When the ratio of cyclones per day for each month is computed the minimum in February is smoothed (figure not shown). Therefore, the decrease in the cyclone frequency from January to February is due to February having fewer days (28 or 29), which affects the count of systems. These results are consistent with climatologies obtained for present and future climates (Hoskins and Hodges 2005, Reboita *et al* 2015, Marrafon *et al* 2021, 2022). Some of the results from figure 1 are also evident in figure 2: a decrease in the frequency of cyclones towards the end of the century, but with a weaker decrease under SAI scenarios (figure 2(b)).

### 3.3. Spatial pattern

In this section, the spatial pattern of extratropical cyclones characteristics (figures 3–6) is presented in terms of comparisons between the future and the reference period, as well as between no-SAI and SAI scenarios.

The future timeslices under no-SAI scenarios indicate a decrease in the SD frequency, mainly in mid-latitudes, and an increase around Antarctica compared to the reference period (figures 3(a), (c), (g), (i) and (m)), which is known in the literature as the poleward shift of the storm tracks under global warming scenarios (Mbengue and Schneider 2013, Chemke 2022). In $GeoMIP_{SSP5-8.5}$ (figures 3(a) and (c)) the decrease is more pronounced than in the other datasets near the continents (southeastern South America, and southern Africa and Australia). These patterns become stronger towards the end of the century (figure 3(c)). SAI scenarios also project a decrease in SD compared to the reference period, but this decrease is lower than that under no-SAI scenarios (figures 3(b), (d), (h), (j) and (n)), which compensates for the effect of global warming. This is clearer in the difference between SAI and no-SAI scenarios, where positive differences (indicative of higher SD under SAI scenarios) predominate mainly around Antarctica and in the latitudes of eastern Australia (figures 3(e), (f), (k), (l) and (o)). $GLENS_{SAI}$ shows an increase in the SD over the South Pacific compared to the reference period (figures 3(h) and (j)). This signal is weak in $GeoMIP_{SAI}$ and only appears in eastern Australia. Hence, the positive SD in GLENS is in general opposite between SAI and no-SAI scenarios, therefore affecting patterns of the other analyzed variables. This different signal in

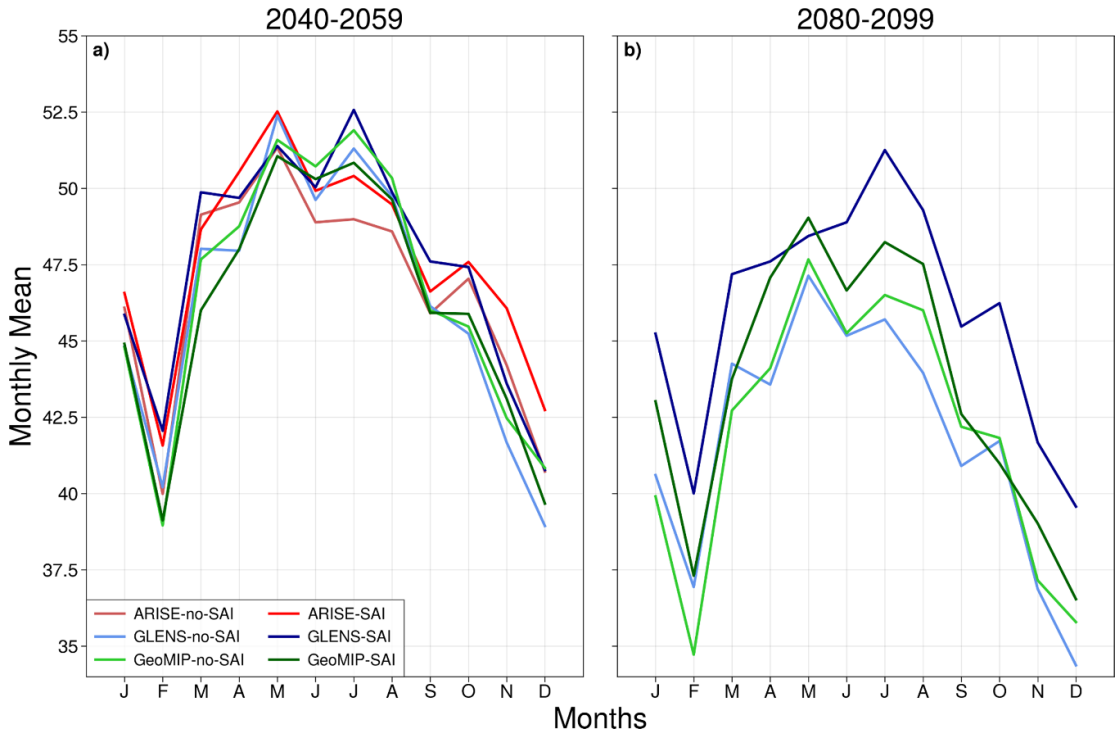


**Figure 2.** Annual cycle of the frequency of extratropical cyclones under no-SAI and SAI scenarios considering (a) 2040–2059 and (b) 2080–2099 periods.

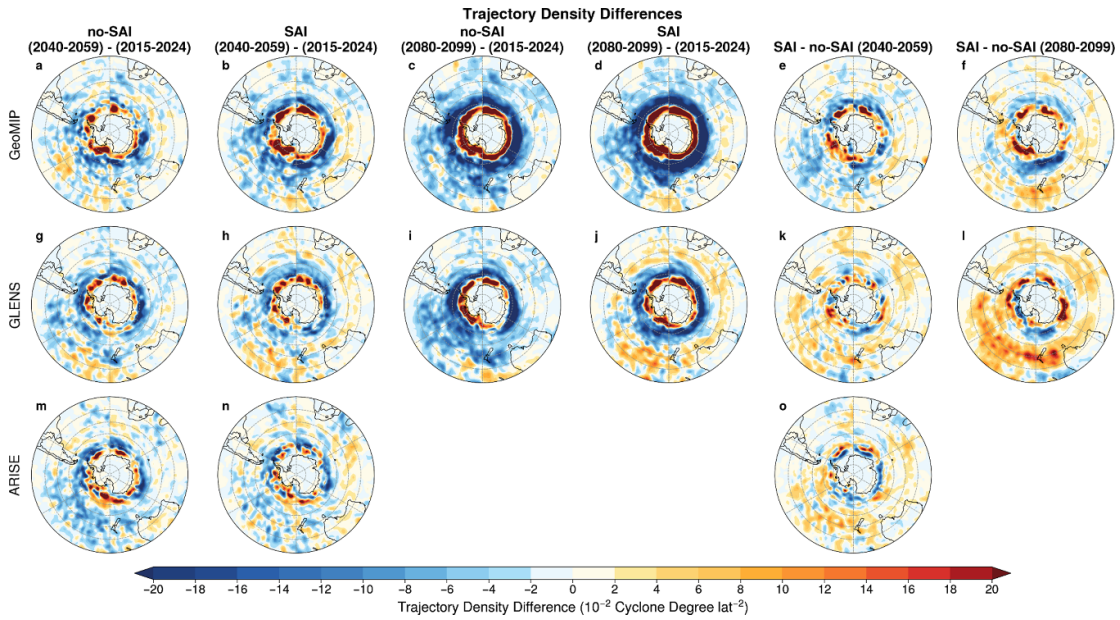


**Figure 3.** Cyclone tracking density (SD) projections for each project (GeoMIP/G6sulfur, GLENS and ARISE). The first to fourth columns indicate the difference between each timeslices and the reference period for (a), (c), (g), (i), (m) no-SAI and (b), (d), (h), (j), (n) SAI scenarios, and the fifth and sixth columns indicate the difference between SAI and no-SAI scenarios.

$GLENS_{SAI}$ might be related with the spreading of aerosols in this projection, which has largest concentrations of sulfate in the tropical band of the Northern Hemisphere (Richter *et al* 2022), and their response to the atmospheric circulation. In this SAI scenario, Bednarz *et al* (2022) found a strengthening of the stratospheric zonal winds that extends downwards to the troposphere, resulting in a poleward shift of the eddy-driven jet and sea-level pressure anomalies, corresponding to the positive phase of the Southern Annular Mode (SAM). According to Reboita *et al* (2015), SAM positive phase is related with a tri-pole in the spatial distribution of cyclones: higher frequency near Antarctica and northward 45S and lower frequency between these two bands. On the other hand, Bednarz *et al* (2022) also indicated an opposite response in $ARISE_{SAI}$ (which has

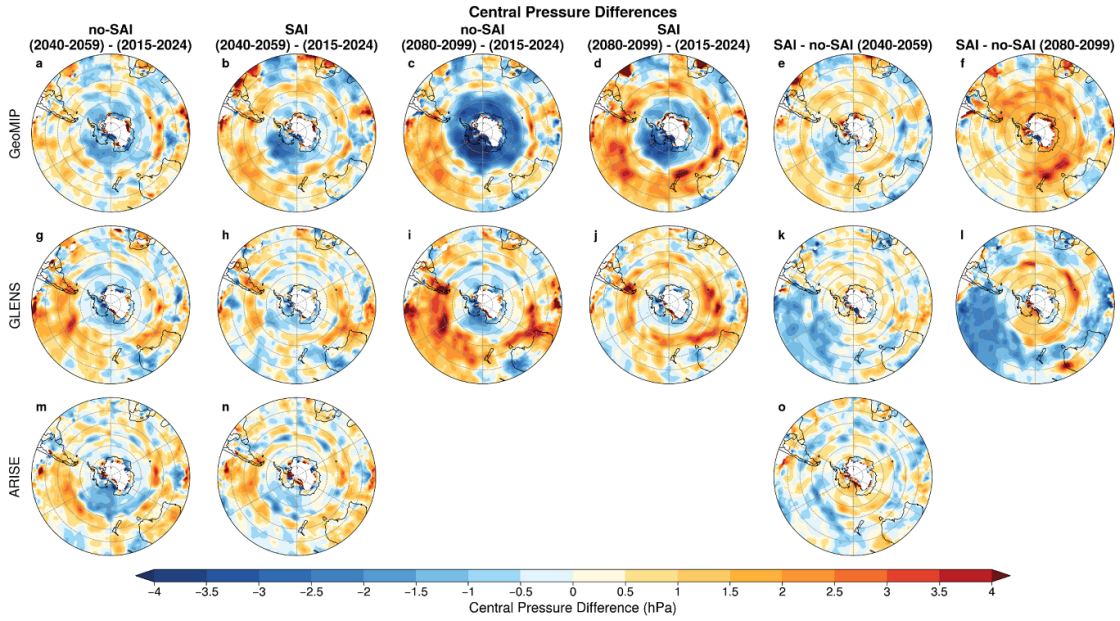


**Figure 4.** Similar to figure 3 but for cyclone central pressure (CP in hPa).

largest concentration of aerosol in the tropics of the Southern Hemisphere), that is, an equatorward shift of the eddy-driven jet and a sea-level pressure response resembling a negative phase of SAM that can make difficult the occurrence of cyclones northward 45S (Reboita *et al* 2015).

Figure 1(c) showed a general view of the MSLP trends in the cyclone's center in the Southern Hemisphere, but in a spatial analysis not the whole hemisphere may present the same CP trend signal. Indeed, both no-SAI (figures 4(a), (c), (g), (i), (m)) and SAI (figures 4(b), (d), (h), (j), (n)) scenarios project stronger systems southern 50S, i.e. towards Antarctica (negative difference in the figures), and weaker in mid-latitudes and near the continental coasts (positive difference). However, there is a difference in SAI compared to no-SAI scenarios: while the increase in intensity of the systems (negative difference) is lower under SAI than under no-SAI scenarios, the decrease in the intensity (positive difference), in general, is higher. This means that, on average, SAI scenarios project weaker systems. Of course there are differences among the projects. For instance, $GLENS_{SAI}$ projects lower MSLP over the Pacific Ocean than $GLENS_{RCP8.5I}$, and also in comparison with $GeoMIP_{SSP5\text{-}8.5/SAI}$. This is a consequence of higher frequency of cyclones projected by $GLENS_{RCP8.5SAI}$ over this ocean, which impacts the MSLP (figures 4(e), (f), (k), (l) and (o)).

As cyclones are perturbations superimposed on a background of the global pressure field, which is characterized by a MSLP decrease from lower to higher latitudes (Sinclair 1994), it is expected cyclones with higher CP (weaker systems) in lower latitudes than in higher latitudes. Due to this fact, the real intensity of the cyclone can be masked when CP is analyzed. A more realistic measure of cyclone intensity is obtained through DP. It should be noted that weaker (stronger) cyclones have lower (higher) DP values; therefore, the DP differences in figure 5 will have opposite signals to CP in figure 4. Despite the previous consideration, when comparing both variables under no-SAI and SAI scenarios, we find good agreement between the spatial distribution of regions with more intense systems and weaker ones. But, a difference occurs between DP and CP over the South Pacific: the CP field shows a larger area with weaker cyclones than DP (for instance in figures 5(a), (c), (g), (i) and (m)). This may be related to the fact that the global pattern of pressure is projected to change in the future, as indicated by various studies suggesting a polar amplification of the Hadley cell, leading to higher pressures towards mid-latitudes (Reboita *et al* 2019 and their references). So, this background is being added to the cyclones environment leading to systems with higher MSLP values. However, in terms of real intensity, there are no great changes in DP over the South Pacific. In a nutshell, the DP confirms that in both future timeslices, extratropical cyclones can be weaker under SAI than no-SAI scenarios (figures 5(e), (f), (k), (l) and (o)).

No-SAI and SAI scenarios practically do not indicate great changes in the R0 in the areas with an increase in DP near Antarctica, but project a decrease in mid-to-low latitudes for the period 2040–2059 (figure 6). A signal of increasing R0 towards Antarctica and near the continents is projected for the period 2080–2099, mainly in southeastern South America, meaning slightly bigger cyclones in future. In general, SAI scenarios project cyclones with slightly lower R0 than the no-SAI scenarios (figures 6(e), (f), (k), (l) and (o)).

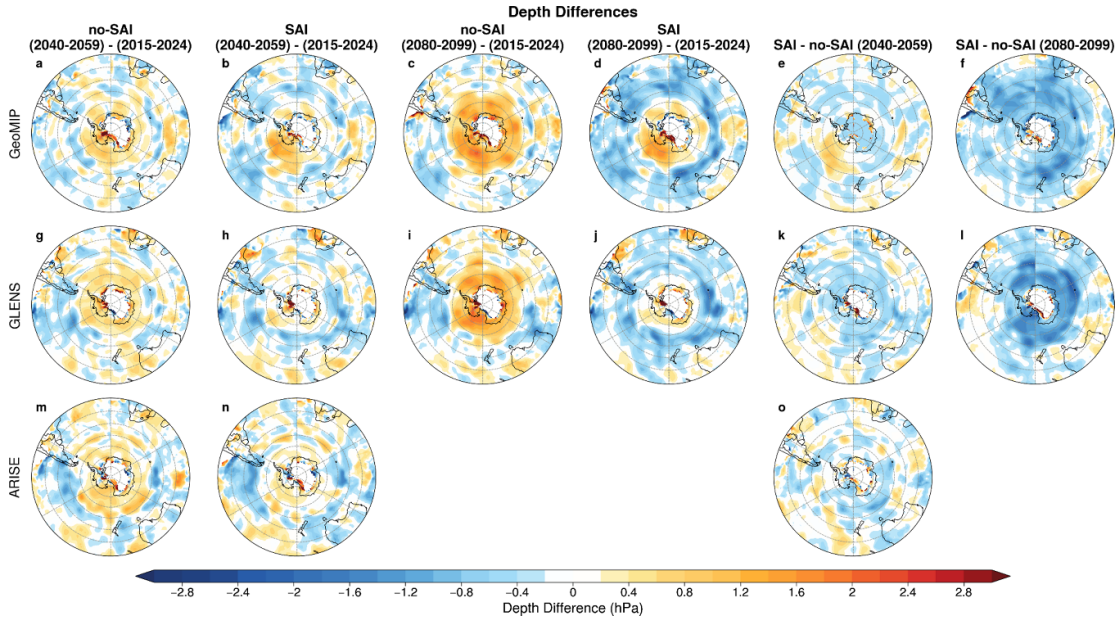


**Figure 5.** Similar to figure 3 but for cyclone depth (DP in hPa).

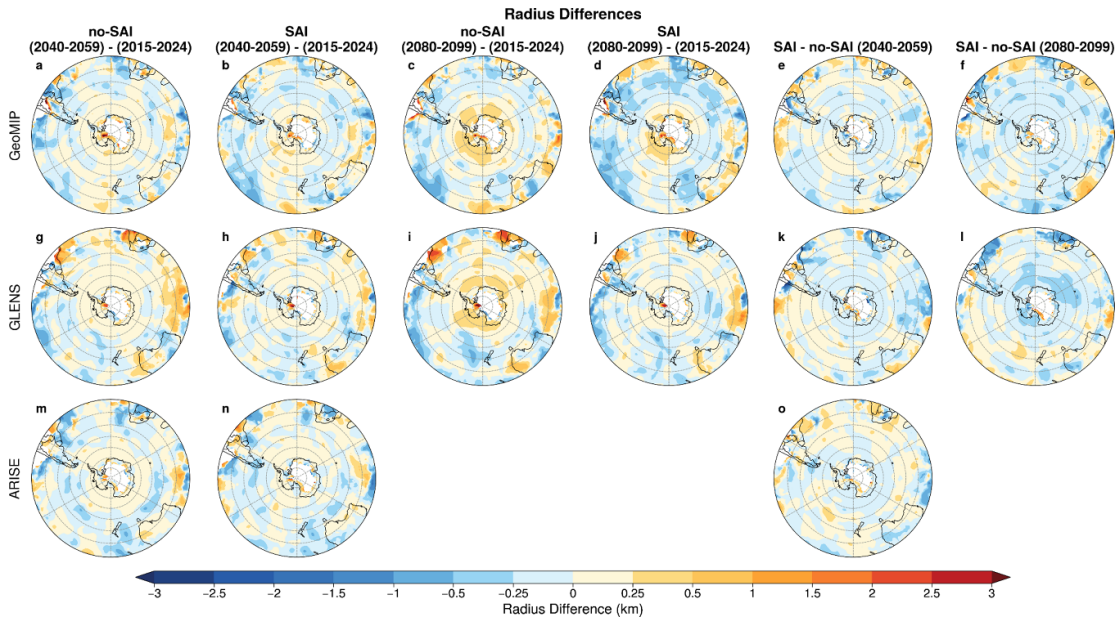


**Figure 6.** Similar to figure 3 but for cyclone radius (R0 in km).

## 4. Conclusions

This study compared the impact of global warming in scenarios with and without stratospheric aerosol injection (SAI and no-SAI, respectively) on extratropical cyclone characteristics over the Southern Hemisphere using projections from three projects: ARISE, GLENS, and GeoMIP/G6sulfur. Despite differences in the projection configuration of the three projects, both no-SAI and SAI scenarios indicate trends in cyclone climatology in the same direction, giving confidence to the results. The main features in the extratropical cyclone climatology are summarized as follows:

*Frequency and annual cycle:* both no-SAI and SAI scenarios for present and future climate exhibit an annual cycle of extratropical cyclone frequency in phase with that described in the literature, with winter being the most cyclogenetic season. The frequency of cyclones decreases towards the end of the century, but with a weaker decrease under SAI scenarios. Therefore, SAI scenarios compensate for the lower frequency of cyclones in the global warming scenario (no-SAI).

*Intensity:* the intensity of extratropical cyclones under no-SAI and SAI scenarios obtained from different approaches (initial pressure, minimum pressure during the lifecycle, and depth) indicates that cyclones will be stronger at the end of the century. However, under SAI scenarios cyclones are less intense compared with no-SAI, highlighting that under SAI cyclones have more similar intensity to the reference period.

*Traveling distance, lifecycle and mean velocity*: there are small differences between the reference period and the end of the century under both no-SAI and SAI scenarios. In addition, the differences between these scenarios are also minimal in the whole studied period.

*Spatial patterns:* although the three projects (ARISE-SAI, GLENS, and GeoMIP/G6sulfur) under both no-SAI and SAI scenarios have some differences in the spatial patterns of cyclone features (trajectory density, central pressure, depth, and radius), they agree that the extratropical cyclones are decreasing (increasing) in density and intensity in mid-latitudes (towards Antarctica), which is a poleward shift of the storm tracks. In addition, they show that the radius of the cyclones can be smaller mainly in mid-to-low latitudes and bigger around Antarctica.

As this is the first study to address SAI in cyclones' climatology—from the tracking perspective—there are no other studies for comparison. However, all described features concerning the no-SAI are consistent with the literature (as shown by the references throughout the text) and they bring important information to the decision makers since coastal areas, such as southeastern South America and New Zealand, are vulnerable to more intense systems in the next decades (e.g. floods, heavy rains, etc.). In addition, there is a consistent indication that the cyclone's climatology is less affected by global warming when SAI is considered.

In a subsequent study, we will evaluate cyclone synoptic patterns through composite analysis to elucidate the physical differences of these systems between no-SAI and SAI scenarios, which provide valuable insights in understanding the impacts of SAI on extratropical cyclones: vital systems to the thermal equilibrium of the planet.

## Data availability statement

All datasets used in this study are available online at the links:

ARISE
www.earthsystemgrid.org/dataset/ucar.cgd.cesm2.waccm6.ssp245.atm.proc.3hourly_ave.html
ARISE-SAI
www.earthsystemgrid.org/dataset/ucar.cgd.ccsm4.ARISE-SAI-1.5.atm.proc.3hourly_ave.html
GLENS www.earthsystemgrid.org/dataset/ucar.cgd.ccsm4.GLENS.Control.atm.proc.6hourly_ave.html
GLENS-SAIhttps://www.earthsystemgrid.org/dataset/ucar.cgd.ccsm4.GLENS.Feedback.atm.proc.6hourly_ave.html
GeoMIP
https://esgf-node.llnl.gov/search/cmip6/
G6sulfur
https://view.es-doc.org/?renderMethod=name&project=cmip6&type=cim.2.designing.NumericalExperiment&client=esdoc-url-rewrite&name=g6sulfur

The data that support the findings of this study are openly available at the following URL/DOI: https://esgf-data.dkrz.de/projects/esgf-dkrz/.

## Acknowledgments

The authors would like to thank the meteorological centers that provided the projections used in this study, Melbourne University for the tracking algorithm, and the financial support of the DEGREES Modelling Fund (DMF) of the DEGREES Initiative. Additional support was received by RCO from the Carnegie Corporation of New York under the Grant No. G-21-58838, and the National Research Foundation of South Africa.

## conflict of interest

The authors declare no conflict of interest.

## ORCID iDs

Michelle Simões Reboita https://orcid.org/0000-0002-1734-2395
João Gabriel Martins Ribeiro https://orcid.org/0000-0002-9854-8693
Natália Machado Crespo https://orcid.org/0000-0002-3585-5100

Romaric C Odoulami https://orcid.org/0000-0001-8228-1608
Windmanagda Sawadogo https://orcid.org/0000-0001-7641-4179

## References

AMS. American Meteorological Society 2022 Climate Intervention: a Policy Statement of the American Meteorological Society (available at: www.ametsoc.org/index.cfm/ams/about-ams/ams-statements/statements-of-the-ams-in-force/climate-intervention/) (Accessed 10 January 2024)
Bednarz E M, Visioni D, Richter J H, Butler A H and MacMartin D G 2022 Impact of the latitude of stratospheric aerosol injection on the Southern Annular Mode *Geophys. Res. Lett.* **49** e2022GL100353
Bengtsson L, Hodges K I and Keenlyside N 2009 Will extratropical storms intensify in a warmer climate? *J. Clim.* **22** 2276–301
Camilloni I, Montroull N, Gulizia C and Saurral R I 2022 La plata basin hydroclimate response to solar radiation modification with stratospheric aerosol injection *Front. Clim.* **4** 763983
Catto J L, Ackerley D, Booth J F, Champion A J, Colle B A, Pfahl S and Seiler C 2019 The future of midlatitude cyclones *Curr. Clim. Change Rep.* **5** 407–20
Catto J L and Pfahl S 2013 The importance of fronts for extreme precipitation *J. Geophys. Res. Atmos.* **118** 10791–801
Catto J L, Shaffrey L and Hodges K I 2011 Northern hemisphere extratropical cyclones in a warming climate in the higem high-resolution climate model *J. Clim.* **24** 5336–52
Cerlini P B, Silvestri L D and Saraceni M 2020 Quality control and gap-filling methods applied to hourly temperature observations over central italy *Meteorol. Appl.* **27** e1913
Chand S, Walsh K W, Camargo S, Kossin J, Tory K, Wehner M and Murakami H 2022 Declining tropical cyclone frequency under global warming *Nat. Clim. Change* **12** 655–61
Chemke R 2022 The future poleward shift of southern hemisphere summer mid-latitude storm tracks stems from ocean coupling *Nat. Commun.* **13** 1730
de Jesus E M, da Rocha R P, Crespo N M, Reboita M S and Gozzo L F 2021 Multi-model climate projections of the main cyclogenesis hot-spots and associated winds over the eastern coast of South America *Clim. Dyn.* **56** 537–57
Dykema J A, Keith D W, Anderson J G and Weisenstein D K 2014 Stratospheric controlled perturbation experiment: a small-scale experiment to improve understanding of the risks of solar geoengineering *Phil. Trans. R Soc.* A **372** 20140059
Eisenstein L, Schulz B, Pinto J G and Knippertz P 2023 Identification of high-wind features within extratropical cyclones using a probabilistic random forest—part 2: climatology over europe *Weather Clim. Dyn.* **4** 981–99
Faria L F D, Reboita M S, Mattos E V, Carvalho V S B, Ribeiro J G M, Capucin B C, Drumond A and Paes Dos Santos A P P D 2023 Synoptic and mesoscale analysis of a severe weather event in southern brazil at the end of june 2020 *Atmosphere* **14** 486
Fasullo J T and Richter J H 2022 Scenario and Model Dependence of Strategic Solar Climate Intervention in CESM *Preprint* (https://doi.org/https://doi.org/10.5194/egusphere-2022-779)
Frederiksen C S, Frederiksen J S, Sisson J M and Osbrough S L 2016 Trends and projections of southern hemisphere baroclinicity: the role of external forcing and impact on australian rainfall *Clim. Dyn.* **48** 3261–82
Gentile E S, Zhao M and Hodges K 2023 Poleward intensification of midlatitude extreme winds under warmer climate *npj Clim. Atmos. Sci.* **6** 219
Gertler C G, O'Gorman P A, Kravitz B, Moore J C, Phipps S J and Watanabe S 2020 Weakening of the extratropical storm tracks in solar geoengineering scenarios *Geophys. Res. Lett.* **47** e2020GL087348
Gramcianinov C B, Campos R M, Soares C G and Camargo R D 2020 Extreme waves generated by cyclonic winds in the western portion of the south atlantic ocean *Ocean Eng.* **213** 107745
Grieger J, Leckebusch G C, Raible C C, Rudeva I and Simmonds I 2018 Subantarctic cyclones identified by 14 tracking methods, and their role for moisture transports into the continent *Tellus* A **70** 1454808
Holton J R 2004 *An Introduction to Dynamic Meteorology* 4th edn (Academic) p 535
Hoskins B J and Hodges K I 2005 A new perspective on southern hemisphere storm tracks *J. Clim.* **18** 4108–29
Hueholt D M, Barnes E A, Hurrell J W, Richter J H and Sun L 2023 Assessing outcomes in stratospheric aerosol injection scenarios shortly after deployment *Earth's Future* **11** e2023EF003488
Irvine P J, Emanuel K, He J, Horowitz L W, Vecchi G A and Keith D W 2019 Halving warming with idealized solar geoengineering moderates key climate hazards *Nat. Clim. Change* **9** 295–9
Irvine P J, Kravitz B, Lawrence M G and Muri H 2016 An overview of the earth system science of solar geoengineering *WIREs Clim. Change* **7** 815–33
Jiang J, Cao L, MacMartin D G, Simpson I R, Kravitz B, Cheng W and Mills M J 2019 Stratospheric sulfate aerosol geoengineering could alter the high-latitude seasonal cycle *Geophys. Res. Lett.* **46** 14153–63
Jones A C, Haywood J M, Dunstone N, Emanuel K, Hawcroft M, Hodges K I and Jones A 2017 Impacts of hemispheric solar geoengineering on tropical cyclone frequency *Nat. Commun.* **8** 1382
Karami K, Tilmes S, Muri H and Mousavi S V 2020 Storm track changes in the middle east and north africa under stratospheric aerosol geoengineering *Geophys. Res. Lett.* **47** e2020GL086954
Kendall M G 1975 *Rank Correlation Methods* (Oxford University Press)
Kodama C, Stevens B, Mauritsen T, Seiki T and Satoh M 2019 A new perspective for future precipitation change from intense extratropical cyclones *Geophys. Res. Lett.* **46** 12435–44
Kravitz B, MacMartin D G, Mills M J, Richter J H, Tilmes S, Lamarque J and Vitt F 2017 First simulations of designing stratospheric sulfate aerosol geoengineering to meet multiple simultaneous climate objectives *J. Geophys. Res. Atmos.* **122** 12616–634
Kravitz B, MacMartin D G, Robock A, Rasch P J, Ricke K, Cole J N S and Yoon J 2014 A multi-model assessment of regional climate disparities caused by solar geoengineering *Environ. Res. Lett.* **9** 074013
Krishnamohan K-P S-P, Bala G, Cao L, Duan L and Caldeira K 2019 Climate system response to stratospheric sulfate aerosols: sensitivity to altitude of aerosol layer *Earth Syst. Dyn.* **10** 885–900
Kumar T V L, Durga G P, Aravindhavel A, Barbosa H A and Rao D N 2022 Analysis of tropospheric warming and stratospheric cooling in the present and future climate from the suite of cmip6 models *Theor. Appl. Climatol.* **149** 1717–26
Lim E and Simmonds I 2002 Explosive cyclone development in the southern hemisphere and a comparison with northern hemisphere events *Mon. Weather Rev.* **130** 2188–209

MacMartin D G, Visioni D, Kravitz B, Richter J H, Felgenhauer T, Lee W R and Sugiyama M 2022 Scenarios for modeling solar radiation modification *Proc. Natl Acad. Sci.* **119** e2202230119
Mann H B 1945 Nonparametric tests against trend *Econometrica* **13** 245–59
Marrafon V H, Reboita M S, da Rocha R P and Crespo N M 2021 Ciclones extratropicais no hemisfério sul: comparação entre diferentes reanálises *Rev. Bras. Climatol.* **28** 48–73
Marrafon V H, Reboita M S, Rocha R P D and Jesus E D 2022 Classificação dos tipos de ciclones sobre o oceano atlântico sul em projeções com o regcm4 e mcgs *Rev. Bras. Climatol.* **30** 1–25
Mbengue C and Schneider T 2013 Storm track shifts under climate change: what can be learned from large-scale dry dynamics *J. Clim.* **26** 9923–30
Michaelis A, Willison J, Lackmann G M and Robinson W A 2017 Changes in winter north atlantic extratropical cyclones in high-resolution regional pseudo–global warming simulations *J. Clim.* **30** 6905–25
Moore J C, Grinsted A, Guo X, Yu X, Jevrejeva S, Rinke A and Ji D 2015 Atlantic hurricane surge response to geoengineering *Proc. Natl Acad. Sci.* **112** 13794–9
Murray R J and Simmonds I 1991a A numerical scheme for tracking cyclone centres from digital data. Part I: development and operation of the scheme *Aust. Meteorol. Mag.* **39** 155–66 (available at: www.bom.gov.au/jshess/docs/1991/murray1.pdf)
Murray R J and Simmonds I 1991b A numerical scheme for tracking cyclone centres from digital data. Part II: application to January and July general circulation model simulations *Aust. Meteorol. Mag.* **39** 167–80 (available at: www.bom.gov.au/jshess/docs/1991/murray2.pdf)
National Research Council 2015 *Climate Intervention: Reflecting Sunlight to Cool Earth* (The National Academies Press)) (https://doi.org/10.17226/18988)
Neu U, Akperov M, Bellenbaum N, Benestad R E, Blender R, Caballero R and Wernli H 2013 Imilast: a community effort to intercompare extratropical cyclone detection and tracking algorithms *Bull. Am. Meteorol. Soc.* **94** 529–47
Niemeier U *et al* 2019 MPI-M MPI-ESM1.2-LR model output prepared for CMIP6 GeoMIP G6sulfur (Earth System Grid Federation) (https://doi.org/10.22033/ESGF/CMIP6.6448)
Patel T D, Odoulami R C, Pinto I, Egbebiyi T S, Lennard C, Abiodun B J and New M 2023 Potential impact of stratospheric aerosol geoengineering on projected temperature and precipitation extremes in South Africa *Environ. Res.: Clim.* **2** 035004
Peixoto J P and Oort A H 1992 Physics of climate *AIP*
Pezza A B and Ambrizzi T 2003 Variability of southern hemisphere cyclone and anticyclone behavior: further analysis *J. Clim.* **16** 1075–83
Pezza A B, Durrant T, Simmonds I and Smith I 2008 Southern Hemisphere synoptic behavior in extreme phases of SAM, ENSO, sea ice extent, and Southern Australia rainfall *J. Clim.* **21** 5566–84
Pezza A B, Rashid H and Simmonds I 2012 Climate links and recent extremes in antarctic sea ice, high-latitude cyclones, southern annular mode and enso *Clim. Dyn.* **38** 57–73
Priestley M D K and Catto J L 2022 Future changes in the extratropical storm tracks and cyclone intensity, wind speed, and structure *Weather Clim. Dyn.* **3** 337–60
Reboita M S, Ambrizzi T, Silva B A, Pinheiro R F and Rocha R P D 2019 The south atlantic subtropical anticyclone: present and future climate *Front. Earth Sci.* **7** 8
Reboita M S, Crespo N M, Torres J A, Reale M, Rocha R P D and Coppola E 2021b Future changes in winter explosive cyclones over the southern hemisphere domains from the cordex-core ensemble *Clim. Dyn.* **57** 3303–22
Reboita M S, Reale M, Rocha R P D, Giorgi F, Giuliani G, Coppola E and Cavazos T 2021a Future changes in the wintertime cyclonic activity over the cordex-core southern hemisphere domains in a multi-model approach *Clim. Dyn.* **57** 1533–49
Reboita M S, Rocha R P D, Ambrizzi T and Gouveia C D 2015 Trend and teleconnection patterns in the climatology of extratropical cyclones over the southern hemisphere *Clim. Dyn.* **45** 1929–44
Richter J H, Visioni D, MacMartin D G, Bailey D A, Rosenbloom N, Dobbins B and Lamarque J 2022 Assessing responses and impacts of solar climate intervention on the earth system with stratospheric aerosol injection (arise-sai): protocol and initial results from the first simulations *Geosci. Model. Dev.* **15** 8221–43
Ricke K, Wan J, Saenger M and Lutsko N J 2023 Hydrological consequences of solar geoengineering *Annu. Rev. Earth Planet. Sci.* **51** 447–70
Robock A, Marquardt A, Kravitz B and Stenchikov G L 2009 Benefits, risks, and costs of stratospheric geoengineering *Geophys. Res. Lett.* **36** L19703
Rocha R P, Sugahara S and Silveira R B D 2004 Sea waves generated by extratropical cyclones in the south atlantic ocean: hindcast and validation against altimeter data *Weather Forecast.* **19** 398–410
Schemm S and Röthlisberger M 2024 Aquaplanet simulations with winter and summer hemispheres: model setup and circulation response to warming *Weather Clim. Dyn.* **5** 43–63
Simmonds I, Keay K and Lim E 2003 Synoptic activity in the seas around antarctica *Mon. Weather Rev.* **131** 272–88
Simmonds I and Murray R J 1999 Southern extratropical cyclone behavior in ecmwf analyses during the frost special observing periods *Weather Forecast.* **14** 878–91
Simmonds I, Murray R J and Leighton R M, 1999 A refinement of cyclone tracking methods with data from FROST *Aust. Meteorol. Mag.* 35–49 (available at: www.bom.gov.au/jshess/docs/1999/simmonds.pdf) (Accessed 14 Feburay 2024)
Sinclair M R 1994 An objective cyclone climatology for the southern hemisphere *Mon. Weather Rev.* **122** 2239–56
Sinclair V A, Rantanen M, Haapanala P, Räisänen J and Järvinen H 2020 The characteristics and structure of extra-tropical cyclones in a warmer climate *Weather Clim. Dyn.* **1** 1–25
Tebaldi C, Debeire K, Eyring V, Fischer E M, Fyfe J C, Friedlingstein P and Ziehn T 2021 Climate model projections from the scenario model intercomparison project (ScenarioMIP) of CMIP6 *Earth Syst. Dyn.* **12** 253–93
Tilmes S, Richter J H, Kravitz B, MacMartin D G, Mills M J, Simpson I R and Ghosh S S 2018 Cesm1(waccm) stratospheric aerosol geoengineering large ensemble project *Bull. Am. Meteorol. Soc.* **99** 2361–71
Vecchi G A and Soden B J 2007 Increased tropical atlantic wind shear in model projections of global warming *Geophys. Res. Lett.* **34** L08702
Visioni D, MacMartin D G, Kravitz B, Boucher O, Jones A, Lurton T and Tilmes S 2021 Identifying the sources of uncertainty in climate model simulations of solar radiation modification with the g6sulfur and g6solar geoengineering model intercomparison project (GeoMIP) simulations *Atmos. Chem. Phys.* **21** 10039–63

Wahab M A 2017 Interpolation and extrapolation *Topics in System Engineering Winter Term* vol 17 pp 1–6 (available at: www.researchgate.net/profile/Muhammad-Wahab-5/publication/313359516_Interpolation_and_Extrapolation/links/58973f6aaca2721f0dae1092/Interpolation-and-Extrapolation.pdf) (Accessed 10 January 2024)

Walker E, Mitchell D and Seviour W J M 2020 The numerous approaches to tracking extratropical cyclones and the challenges they present *Weather* **75** 336–41

Walsh K, McBride J L, Klotzbach P J, Balachandran S, Camargo S J, Holland G J and Sugi M 2015 Tropical cyclones and climate change *WIREs Clim. Change* **7** 65–89

Wieners K *et al* 2019 MPI-M MPI-ESM1.2-LR model output prepared for CMIP6 CMIP historical (Earth System Grid Federation) (https://doi.org/10.22033/ESGF/CMIP6.6595)

Wilks D S 2020 *Statistical Methods in the Atmospheric Sciences* 4th edn (Elsevier) p 840

Xu D, Cao D and Wang D 2023 The change of southern hemisphere extratropical cyclone precipitation characteristics in ssp5-8.5 scenario in cmip6 models *Clim. Dyn.* **61** 2443–56